Laser and Particle Beams (2002), *20*, 67–72. Printed in the USA.
Copyright © 2002 Cambridge University Press 0263-0346/02 $12.50
DOI: 10.1017.S0263034602201093

Femtosecond, picosecond, and nanosecond laser microablation: Laser plasma and crater investigation

A. SEMEROK,[1] B. SALLÉ,[1] J.-F. WAGNER,[1] AND G. PETITE[2]
[1]CEA Saclay, DPC/SCPA/LALES, Bât.391, 91191 Gif sur Yvette Cedex, France
[2]DSM/DRECAM/LSI, Ecole Polytechnique, 91128 Palaiseau Cedex, France

(RECEIVED 28 March 2001; ACCEPTED 16 October 2001)

Abstract

Crater shapes and plasma plume expansion in the interaction of sharply focused laser beams (10 μm waist diameter, 60 fs–6 ns pulse duration) with metals in air at atmospheric pressure were studied. Laser ablation efficiencies and rates of plasma expansion were determined. The best ablation efficiency was observed with femtosecond laser pulses. It was found that for nanosecond pulses, the laser beam absorption, its scattering, and its reflection in plasma were the limiting factors for efficient laser ablation and precise material sampling with sharply focused laser beams. The experimental results obtained were analyzed with relation to different theoretical models of laser ablation.

Keywords: Laser ablation; Laser plasma; Metal samples

1. INTRODUCTION

The interaction of a powerful laser beam with a solid sample results in a crater formation on the sample surface and the creation of laser plasma that is composed of excited atoms and ions of the sample. This plasma is of analytical interest for solid surface characterization (elemental cartography or mapping) by spectral analysis of the plasma emission (method of laser ablation/optical emission spectroscopy). Spatial resolution of this method is associated with the crater dimensions that are determined not only by the laser beam waist, but by the laser beam interaction with the sample surface and the near surface plasma as well. The interaction is a complex process involving heating, melting, evaporation, excitation, and ionization. It has not yet been satisfactorily explained and is still under intensive investigation (Mele *et al.*, 1997; Mao *et al.*, 1998; Sallé *et al.*, 1999; Semerok *et al.*, 1999). It depends on a great number of laser–matter interaction parameters such as laser pulse duration, wavelength, angular divergence, spot size and energy, physical properties of solid matter, surrounding environment composition, and pressure. Such a multiparameter dependence of the interaction process presents difficulties both for theoretical analysis of the ablation process and the interpretation of experimental results and obtained dependencies.

Address correspondence and reprint requests to: A. Semerok, CEA Saclay, DPC/SCPA/LALES, Bât. 391, 91191 Gif sur Yvette Cedex, France. E-mail: asemerok@cea.fr

The aim of this work was to investigate the crater shapes and the microplasma expansion in the interaction of laser pulses (60 fs–6 ns pulse duration) with pure metals. For this range of laser pulse duration, different regimes of laser ablation can be studied. They are defined by the characteristic time of electron–phonon interaction in solids (of the order of 1 ps; Anisimov & Rethfeld, 1996; Momma *et al.*, 1997) and correspond to the ablation with laser–plasma interaction (for ns/ps pulses) and without it (for fs pulses). Laser–plasma interaction can change dramatically both the laser beam intensity distribution on the solid surface and the laser plume expansion features. The investigation of the laser plasma limiting effects in nanosecond laser microablation was under study as well.

2. EXPERIMENT

The experiments were carried out with two different lasers in air at atmospheric pressure. A set of metal samples (Cu, Al, and Pb) with various material parameters (Semerok *et al.*, 1998) was chosen to investigate the effect of material properties on the laser ablation process. The surfaces were polished to facilitate the localization of the microcraters and to increase the accuracy of crater parameters measurements.

The nanosecond pulse experiments were performed with a Nd-YAG laser (Quantel Compact YG 585) with a 6 ns (FWHM) pulse duration emitting on the first (1064 nm), second (532 nm), or fourth (266 nm) harmonic. The laser

https://doi.org/10.1017/S0263034602201093 Published online by Cambridge University Press

beams with near the Gaussian intensity distribution were focused by a 100 mm lens at normal incidence to the sample surface. The waist diameters were found to be 10 μm (FWHM of intensity distribution) for 1064 nm and 532 nm and 6 μm for 266 nm. The laser beam energy was varied in the range of 0.01 mJ $\leq E \leq$ 4 mJ (10 J/cm^2 $\leq F \leq$ 4500 J/cm^2).

The femtosecond–picosecond experiments were performed with Ti-Al_2O_3 laser emitting on the first (800 nm), second (400 nm), or third (266 nm) harmonic. The laser beams with wavelengths of 800 nm or 400 nm were focused by a 150-mm lens at normal incidence to the metal sample surface. A 200-mm lens was used for the 266-nm laser beam. The waist diameters were found to be close to 10 μm (FWHM of the intensity distribution) for all laser beams. The laser pulse duration was adjusted in the 70 fs–10 ps range. The laser energy was varied in the range of 2 μJ $\leq E \leq$ 800 μJ (2 J/cm^2 $\leq F \leq$ 800 J/cm^2).

The craters formed at the surfaces were studied with an optical microscope profilometer (MicroXam Phase Shift Technology, USA) of 1 μm lateral and 0.01 μm longitudinal resolutions. The laser plasma images were obtained by means of an intensified gated CCD camera (Hamamatsu C4346-01) with a 3-ns gate time. At the first stage of the laser plasma expansion, the time delay with a 1-ns step was applied. A microscope objective of 40× magnification was used for the laser plasma imaging with 3-μm lateral resolution. Thus, laser plasma expansion was measured with 3-μm spatial and 1-ns time resolutions. These measurements were performed in a time delay range of 0 to 100 ns and at different wavelengths in a spectral range of 200 to 850 nm. Other objectives of 12.5× and 2.5× magnification were used for laser plasma imaging at the time delay range of 40 to 500 ns and 500 to 1000 ns, where plasma dimensions reached up to 1000 μm.

3. EXPERIMENTAL RESULTS

Figure 1 gives the typical crater profile obtained in our experiments with nanosecond laser pulses. On the target surface along the crater boundary we observed formation of a convexity, the height of which depended on the target material, pulse duration, energy, and pulse number. With the pulse number increased, the ratio of the convexity height (δ) to the crater depth (h) decreased. The crater diameters $D_{0.5}$ and D_m usually followed the laser beam diameter, but depended on pulse energy, laser wavelength, and target material as well. For femtosecond pulses, the crater profiles were without convexity formation. In general, the crater profiles were not identical to the spatial distribution of laser intensity. Only at the lowest energy was the crater shape observed to coincide with the laser intensity distribution of femtosecond pulses (any wavelength) and nanosecond–picosecond pulses (for the second and fourth harmonics). For nanosecond pulses on 1064 nm, the crater diameters $D_{0.5}$ were smaller than laser beam diameter. At higher energies, the crater diameters were found to be larger than diameters of laser beam for all wavelengths and pulse durations. Figure 2 gives the dependences of crater diameters $D_{0.5}$ and D_m on the incident laser energy (532 nm, 6 ns) for copper. In the 0.01–1 mJ range, the surface diameter increased significantly from an initial 15 μm to about 45 μm. Then, for energies higher than 1 mJ, the diameter reached approximately the same value of around 50 μm. The crater diameter $D_{0.5}$ demonstrated a particular behavior with the laser pulse energy. It increased from 10 μm at 0.01 mJ up to 20 μm at 0.1 mJ. Then, it fell to a constant value of around 18 μm. These data indicate that the crater shape varied with the laser energy. Up from 0.2 mJ, the profile of the crater suffered crucial changes—a large shallow area of erosion could be observed around the main deep crater. In our experiments, the crater depth and volume were observed to increase with laser fluence and energy, respectively (Figs. 3 and 4). The crater behavior presented for copper was similar to all metals under investigation. The differences observed were attributed to ablation efficiencies. For a 532-nm, 6-ns laser beam, they were found to be 5000 μm^3/mJ, 2000 μm^3/mJ, and 6000 μm^3/mJ for Al, Cu, and Pb, respectively. In the 0.01–0.06 mJ energy range, the ablation efficiency for copper was the same for all nanosecond-laser wavelengths. With the pulse energies higher at 0.06 mJ, the ablation was more efficient for short wavelengths.

The craters formed with different Ti-Al_2O_3 laser pulse durations were of a similar typical profile. No convexity was observed on the target surface around the crater. The crater depth per pulse versus laser pulse duration is shown in

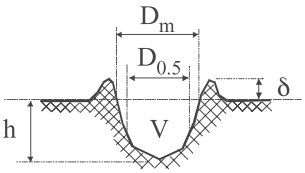

Fig. 1. Crater spatial characteristics.

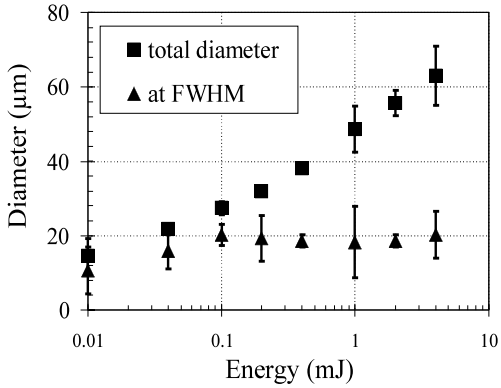

Fig. 2. Dependence of crater diameter on incident laser energy (532 nm, 6 ns) for copper.

https://doi.org/10.1017/S0263034602201093 Published online by Cambridge University Press

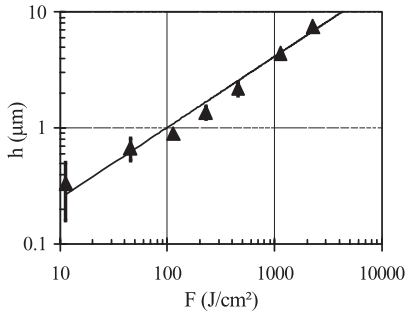

Fig. 3. Dependence of crater depth on laser fluence (532 nm, 6 ns) for copper after one laser shot. Solid line is fitting curve $h\ (\mu\text{m}) = 0.06F^{0.6}$ (J/cm^2).

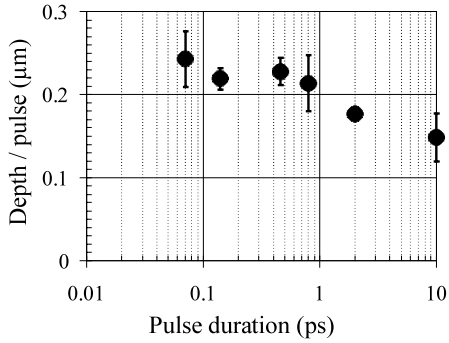

Fig. 5. Laser ablation efficiency for different pulse durations of Ti:Al_2O_3 laser. Laser wavelength—800 nm, target—Cu, energy—20 μJ.

Figure 5. No significant changes in crater depth were observed in the 70–800 fs range. For higher pulse durations, the crater depth decreased with laser pulse duration increase. The same behavior was observed for crater volume versus laser pulse duration. This is in good agreement with our previous experimental results (Semerok *et al.*, 1999). Femtosecond-laser ablation efficiency (2000 μm^3/mJ for Cu) was found to be independent of the laser wavelength for 70-fs pulses.

The plasma expansion was studied for a copper target with 532-nm nanosecond pulses. For short delay times (0–20 ns) a more intense area on the sample surface level disappears when a 515-nm filter, which cuts off laser wavelength, is used. This intensity, being stronger than the one of the plasma emission, is attributed, consequently, to the laser beam diffusion on the target surface. At 0.1 mJ energy, the ablated vapor escapes the surface with fast expansion in the normal direction of the target. At the end of the laser pulse, the plasma comes unstuck from the surface and takes the shape of a mushroom. An intense plasma core is located near the surface with the maximum intensity observed at a certain distance from the surface. Then, the intensity decreases until it reaches its minimum. It increases again until the maximum is reached at a distance of around 75 μm above the sample surface. For longer delay times, the emission near the surface disappears and the plasma volume does not evolve any more. This kind of plasma behavior is observed in the energy range of 0.01 to 0.4 mJ. At 1-mJ energy, the rate of the plasma expansion is higher. An additional cone-shaped plume is detected in this case. The formation of this cone-shaped plume is observed for plasmas created with energies higher than 0.4 mJ. For short delay times, highly intense "hot spots" can be seen in the plume along the laser beam path. The width of these hot spots is measured to be close to the laser beam diameter (10 μm). With a 515-nm filter, the plasma created by 1-mJ pulses does not exhibit any intense hot spots. A similar observation was made with the filters being transmitted in the ranges of $250 < \lambda < 400$ nm and $600 < \lambda < 800$ nm. Thus, we may conclude that the hot spots are not associated with a higher concentration of the excited copper atoms in these areas, but they are rather attributed to scattering of the laser beam in the plasma plume. The dimensions of the plasma were measured at the maximum plasma intensity divided by 10. This intensity level was considered as the plasma plume boundary. The temporal evolution of longitudinal dimension of plasmas created on aluminum, copper, and lead samples at 1 mJ is presented in Figure 6. The plasma begins to grow very quickly during the first 50 ns and the expansion does not depend on the ablated material. The plume reaches the max-

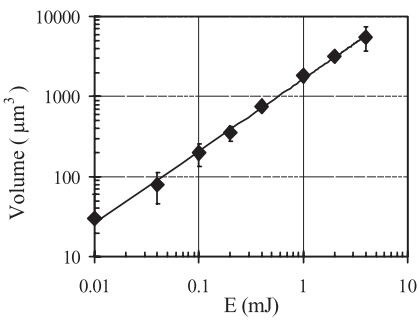

Fig. 4. Dependence of crater volume on laser energy (532 nm, 6 ns) for copper. Solid line is fitting curve $V\ (\mu\text{m}^3) = 1650E^{0.9}$ (mJ).

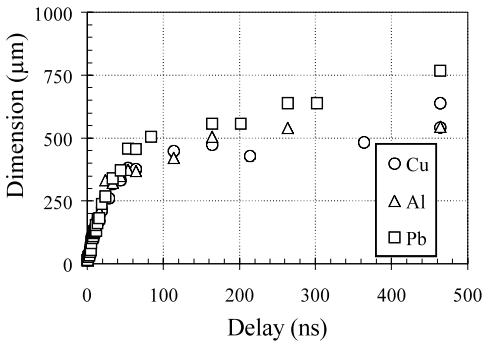

Fig. 6. Temporal evolution of longitudinal dimension of plasma created on aluminum, copper, and lead for 1-mJ laser pulses (532 nm, 6 ns).

https://doi.org/10.1017/S0263034602201093 Published online by Cambridge University Press

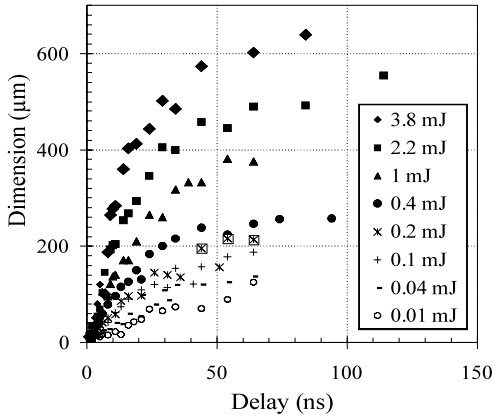

Fig. 7. Temporal evolution of the longitudinal copper plasma dimension for 0.01–4 mJ laser pulse energies (532 nm, 6 ns).

imum dimensions at 500 ns delay, then no further changes are observed. The most efficiently ablated material (Pb) was observed to have the largest plasma volume. When the energy increases, the initial expansion rate and the maximum plasma volume grow (Fig. 7). Nevertheless, the character of the temporal evolution of the plasma dimensions is the same for all the energies.

For different pulse durations and wavelengths of Ti-Al_2O_3 laser, the plasma exhibits a similar spatial evolution. The temporal evolution of the plasma longitudinal dimension is given in Figure 8. The plasma transversal dimension has the same typical temporal evolution. During the first nanoseconds, the ablated matter escapes the surface with a fast expansion in the normal direction to the target. The initial rates of expansion do not depend significantly on the laser pulse duration. Longitudinal and transversal rates of expansion for 20-μJ laser pulses are found to be about 4.6×10^5 cm/s and 3×10^5 cm/s, respectively. These values are close to the sound velocity in the copper target. From 25-ns delays and upward, the plasma volume does not expand any more, but depends on the laser pulse duration.

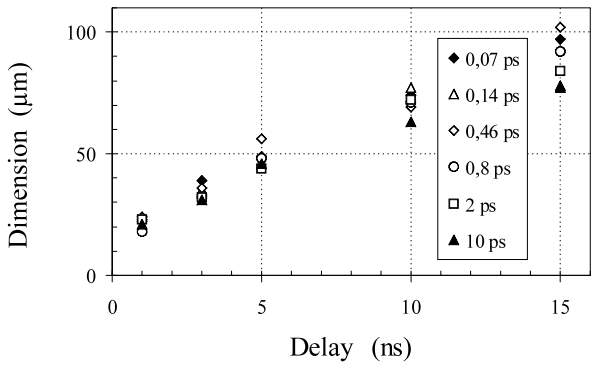

Fig. 8. Temporal evolution of the longitudinal copper plasma dimension obtained with different 800 nm pulse durations. Laser pulse energy—20 μJ.

4. DISCUSSION

Knowledge of the plasma dimension evolution (Fig. 7) allows us to estimate the longitudinal and transversal expansion velocities at the beginning of plume expansion (Table 1). For $E < 0.4$ mJ, the longitudinal expansion velocity was determined to be lower than the transversal one. Above 0.4 mJ, the plasma is cone-shaped and the longitudinal velocity becomes higher than the transversal one. Additional experiments with the incident angle of 45° demonstrated that this cone-shaped plume follows the direction of the Nd-YAG laser beam even though the plasma near the sample expands in the normal direction to the target. This observation implies that the cone-shaped plume is driven by the plasma absorption of the laser light, resulting in a laser-supported ionization wave in air. The plasma plume "expansion" velocity v_p can be simulated by the "absorption wave" model (Berchenko *et al.*, 1979). In this model, the energy balance can be described as (Radziemski & Cremer, 1989): $I \cong \alpha\sigma T^4 + v_p(cT + E_i)$, where α is a coefficient of plasma grayness, σ is the Stephan–Boltzmann constant, $I(\mathrm{W \cdot cm^{-2}})$ is the laser intensity, $c(\mathrm{J \cdot cm^{-3} \cdot K^{-1}})$ is the specific thermal capacity of air, $T(\mathrm{K})$ is the plasma temperature, and E_i is the specific ionization energy of air. The energy of ionization (E_i) and the thermal capacity (c) should be evaluated by taking into account the degree of ionization (it is about 3 for the plasma temperature $T \approx 10^5\,\mathrm{K}$ /10/) (Zeldovich & Raizer, 1966) and the contribution of free electrons and chemical reactions in air. It makes the numerical evaluation of v_p very difficult. At high plasma temperatures ($T \cong 10^5$–3×10^5 K) and high laser intensities (10–100 GW/cm^2), the velocity of the plasma plume expansion can be estimated from the kinetic theory of electron ionization (Zeldovich & Raizer, 1966) $v_{exp} \cong CkT_e(8kT_e/\pi m)^{1/2}N^{2/3}$, where T_e is the electron temperature of plasma (approximately equal to T), m is the mass of the electrons, N is the concentration of atoms in the initial gas, C is a constant about $0.7–0.85 \times 10^{-17}$ cm^2/eV. The value of v_p in this case is about 10^6 cm/s. This is in a sufficiently good agreement with our experimental data (Table 1). But there are no reasons to use this model when the optical properties of plasma can suffer significant changes due to laser–plasma interaction. For solid matter surface

Table 1. *Longitudinal V_l and transversal V_t velocities of copper plasma versus the incident laser energy E (mJ) at 532 nm.*

E (mJ)	V_l (cm/s)	V_t (cm/s)
0.1	2.3×10^5	3.6×10^5
0.04	4.4×10^5	5.0×10^5
0.1	4.6×10^5	5.7×10^5
0.2	6.0×10^5	8.3×10^5
0.4	9.4×10^5	8.5×10^5
1	1.4×10^6	1.1×10^6
2	2.0×10^6	1.4×10^6
4	2.7×10^6	1.6×10^6

https://doi.org/10.1017/S0263034602201093 Published online by Cambridge University Press

Table 2. *Experimental h_{exp} and theoretical h_{theor} longitudinal dimensions of copper plasma for different energies at 532 nm.*

E (mJ)	h_{exp} (μm)	H_{theor} (μm)
0.01	125	114
0.04	168	181
0.1	217	246
0.2	290	310
0.4	258	390
1	644	529
2	>550	667
4	>620	840

temperature $T > 1$ eV, the crater growth velocity may be determined by the Frenkel (1995) expression: $v_c(T) \cong v_s \exp(E_0/kT)$, where v_s is a velocity close to the sound velocity in solid matter; E_0 is the energy of the atom bond in solid matter; kT is the plasma particles' energy. In this case, the plasma expansion velocity has to be at least equal to or higher than crater growth velocity. Thus, for an ablation regime without a plasma absorption wave (laser energies $0.01 \leq E \leq 0.4$ mJ), the plasma expansion can be estimated by the Frenkel formula. Table 2 compares the experimental values of the maximum longitudinal dimensions of copper plasma for different energies with the theoretical data. The maximum height reached by the plasma front was evaluated by the following expression (Arnold *et al.*, 1999): $R_{\max} \approx 0.39 \times (\eta E/P_0)^{1/3}$, where P_0 is the pressure of ambient gas, and η is the ratio of the plasma plume energy to that of the laser pulse. The experimental results are in good agreement with theoretical values for $\eta = 0.25$ and the laser energies below 0.4 mJ.

The experimentally obtained crater widening and its profile changes with the laser pulse energy increase can be attributed to the scattering and refraction of the laser beam in plasma. The crater widening and crater profile changes were observed at the strong scattering of laser beam in plasma. Thus, our experiments, analogous to the results in Bonch-Bruevich *et al.* (1980), demonstrated that light diffusion and refraction by the plasma plume play a decisive role in laser intensity distribution on the solid surface, resulting in crater broadening and its profile changes.

For the applied range of laser pulse duration, two ablation regimes can be distinguished: below 1 ps, when a nonthermal process take place and above 1 ps, when ablation can be considered as a thermal process (Von der Linde *et al.*, 1997). The ablation efficiency decrease with the pulse duration's increase in the range above 1 ps can be explained by the plasma shielding and refraction of laser radiation and increase of heat conduction losses (Momma *et al.*, 1996). The femtosecond laser ablation efficiency (with the pulse duration less than 800 fs) was found to be independent of the pulse duration. It can be explained within the framework of the femtosecond-laser ablation model (Nolte *et al.*, 1997). The ablation efficiency in this model is characterized by the effective penetration depth that is determined either by the optical penetration depth (at low fluence) or by the heat penetration depth (at high fluence), being independent of the pulse duration as well.

5. CONCLUSIONS

The experimental studies of crater profile and plasma expansion at the interaction of the sharply focused nanosecond laser beam with metal samples demonstrated with certainty the plasma-limiting effects on laser microablation. This was revealed not only by the decrease of crater depth growth with laser energy increase, but by the crater widening and its profile changes as well. The experimentally obtained velocities of plasma plume expansion and the dimensions of the laser plasma plume may be described by the Frenkel (1955) and shock wave (Arnold *et al.*, 1999) models.

Two different regimes of laser–target interaction were identified. The first one is a femtosecond regime, where the laser pulse ends before the energy is completely redistributed in the solid matter. Thus the pulse energy is deposited in the matter without any participation of a laser–plasma interaction. The second regime is a nanosecond–picosecond one, where the laser pulse duration is of the same order or longer than the energy relaxation time. The irradiated volume heating is fast enough to heat and vaporize the surface material during an early stage of laser pulse duration. In this case, the heat conduction losses and the plasma shielding effects reduce the ablation efficiency.

ACKNOWLEDGMENTS

The authors would like to acknowledge Prof. M. Libenson and Dr. N. Arnold for fruitful discussions on laser plasma expansion properties, as well as Mr. J.-L. Lacour, Dr. O. Gobert, Mr. P. Meynadier, and Mr. M. Perdrix for technical assistance.

REFERENCES

Anisimov, S.I. & Rethfeld, B. (1996). On the theory of ultrashort laser pulse interaction with metal. *SPIE*, **3093**, 192–203.

Arnold, N., Gruber, J. & Heitz, J. (1999). Spherical expansion of the vapor plume into ambient gas: an analytical model. *Appl. Phys. A* **69**, S87–S93.

Berchenko, E.A., Sobolev, A.P. & Fedyushin, B.T. (1979). Propagation of laser-absorption waves in a gas. *Sov. J. Quant. Electr.* **9**, 907–908.

Bonch-Bruevich, A.M., Kakabushkin, L.N., Kaporskii, V.S. & Salyadinov, V.S. (1980). Anisotropy in the scattering of light by the plasma of a laser spark. *Sov. Tech. Phys. Lett.* **66**, 289–290.

Frenkel, Y.I. (1955). *Kinetic Theory of Liquids*. New York: Dover Publications, Inc.

Mao, X.L., Ciocan, A.C., Borisov, O.V. & Russo, R.E. (1998). Laser ablation processes investigated using inductively coupled plasma–atomic emission spectroscopy (ICP–AES). *Appl. Surf. Sci.* **127–129**, 262–268.

https://doi.org/10.1017/S0263034602201093 Published online by Cambridge University Press

Mele, A., Giardini-Guidoni, A., Kelly, R., Flamini, C. & Orlando, S. (1997). Laser ablation of metals: Analysis of surface-heating and plume-expansion experiments. *Appl. Surf. Sci.* **109–110**, 584–590.

Momma, C., Chichkov, B.N., Nolte, S., von Alvensleben, F., Tünnermann, A., Welling, H. & Wellegehausen, B. (1996). Short-pulse laser ablation of solid targets. *Opt. Commun.* **129**, 134–142.

Momma, C., Nolte, S., Chichkov, B.N., von Alvensleben, F. & Tünnermann, A. (1997). Precise laser ablation with ultrashort pulses. *Appl. Surf. Sci.* **109–110**, 15–19.

Nolte, S., Momma, C., Jacobs, H., Tünnermann, A., Chichkov, B.N., Wellegehausen, B. & Welling, H. (1997). Ablation of metals by ultrashort laser pulses. *J. Opt. Soc. Am. B* **14**, 2716–2722.

Radziemski, L.J. & Cremer, D.A. (1989). *Laser Induced Plasmas and Applications*. New York: Marcel Dekker.

Sallé, B., Chaléard, C., Detalle, V., Lacour, J.-L., Mauchien, P., Nouvellon, C. & Semerok, A. (1999). Laser ablation efficiency of metal samples with UV laser nanosecond pulses. *Appl. Surf. Sci.* **138–139**, 302–305.

Semerok, A., Chaléard, C., Detalle, V., Kocon, S., Lacour, J.-L., Mauchien, P., Meynadier, P., Nouvellon, C., Palianov, P., Perdrix, M., Petite, G. & Sallé, B. (1998). Laser ablation efficiency of pure metals with femto, pico and nanosecond pulses. *SPIE* **3343**, 1049–1055.

Semerok, A., Chaléard, C., Detalle, V., Lacour, J.-L., Mauchien, P., Meynadier, P., Nouvellon, C., Sallé, B., Palianov, P., Perdrix, M. & Petite, G. (1999). Experimental investigations of laser ablation efficiency of pure metals with femto, pico and nanosecond pulses. *Appl. Surf. Sci.* **138–139**, 311–314.

Von der Linde, D., Sokolowski-Tinten, K. & Bialkowski, J. (1997). Laser–solid interaction in the femtosecond time regime. *Appl. Surf. Sci.* **109–110**, 1–10.

Zeldovich, Ya. & Raizer, Yu. (1966). *Physics of Shock Waves and of High-Temperature Hydrodynamic Effects*. New York, London: Academic Press.

https://doi.org/10.1017/S0263034602201093 Published online by Cambridge University Press